Applied Catalysis B: Environmental 84 (2008) 598–606

Contents lists available at ScienceDirect

Applied Catalysis B: Environmental

journal homepage: www.elsevier.com/locate/apcatb

Photocatalytic degradation of toluene over doped and coupled (Ti,M)O_2 (M = Sn or Zr) nanocrystalline oxides: Influence of the heteroatom distribution on deactivation

Fernando Fresno [a,b,*], María D. Hernández-Alonso [a], David Tudela [b], Juan M. Coronado [c], Javier Soria [a]

[a] Instituto de Catálisis y Petroleoquímica, CSIC, C/Marie Curie 2, Cantoblanco, 28049 Madrid, Spain
[b] Departamento de Química Inorgánica, Facultad de Ciencias, Universidad Autónoma de Madrid, 28049 Madrid, Spain
[c] Aplicaciones Medioambientales de la Energía Solar, CIEMAT. Av. Complutense 22, 28040 Madrid, Spain

ARTICLE INFO

Article history:
Received 10 March 2008
Received in revised form 12 May 2008
Accepted 17 May 2008
Available online 28 May 2008

Keywords:
Photocatalysis
TiO_2
Toluene
VOC's
SnO_2
ZrO_2
Coupled oxides
Mixed oxides
Infrared spectroscopy

ABSTRACT

In this work, we have studied the photocatalytic oxidation (PCO) of toluene over Sn- and Zr-doped TiO_2, and coupled TiO_2/SnO_2 and TiO_2/ZrO_2 catalysts. The TiO_2 sample doped with Sn (8% of metal ions) is composed by the anatase and rutile phases of TiO_2, while the Zr-doped sample (same dopant content) contains only the anatase phase. The coupled photocatalysts are formed, in addition to the phases present in their doped counterparts, by a segregated MO_2 phase (M: Sn or Zr). For the photocatalytic degradation of toluene, higher rates in the stationary state are obtained with the coupled catalysts with respect to the doped ones and the TiO_2 references (both synthetic and Degussa P25). In the case of the coupled photocatalysts, these higher rates are due to the absence of the deactivation that does occur for the rest of samples. Fresh and used photocatalysts have been studied by FTIR and EPR spectroscopies and by solid/liquid extraction in methanol, followed by GC/MS analysis. The obtained results lead us to conclude that, while structural and electronic modifications, due to the guest cations, are responsible for the high activity of doped samples observed in previous studies for a reaction not causing catalyst deactivation (methylcyclohexane PCO), other factors are crucial for the PCO of toluene. For this reaction, there is a relationship between surface water, adsorbed intermediates and resistance to deactivation, and thus the modifications in the amount and arrangement of surface water molecules caused by the second oxide may be the cause of the high degradation rate obtained with the coupled TiO_2/SnO_2 and TiO_2/ZrO_2 photocatalysts.

1. Introduction

Photocatalytic oxidation (PCO) over UV-irradiated semiconductors, among which TiO_2 is by far the most employed one, is one of the so-called Advanced Oxidation Technologies that are aimed to quantitatively transform organic contaminants into their mineralisation products [1,2]. Among the wide variety of pollutants that can be degraded by heterogeneous photocatalysis, volatile organic compounds (VOCs) constitute an important group, given their abundance and their toxicity and environmental damage [3].

Toluene is a major VOC in industrial emissions, indoor air and exhaust gases from motor vehicles, and its PCO has been extensively studied. However, low rates are generally obtained in the toluene photocatalytic degradation reaction due to catalyst deactivation [4–9], which has been generally ascribed to the accumulation of recalcitrant, strongly bound reaction intermediates on the catalyst surface, although some discrepancies exist about the nature of the intermediates responsible for deactivation [10]. Several research groups have investigated the regeneration of the deactivated catalysts after the PCO of toluene and other aromatic compounds by UV-irradiation of the catalyst in a humid air stream [5,8,11,12]. In this respect, water plays an important role in photocatalysis as it contributes to the regeneration of surface hydroxyls that give rise, under irradiation, to the highly oxidative $^{\bullet}OH$ radicals involved in the photocatalytic oxidation of organic compounds. Thus, the presence of water in the reaction medium can partially inhibit deactivation and the observed loss of activity is generally higher in the absence of water vapour [8,11,13,14].

The modification of the characteristics of TiO_2 has been explored as a way to avoid deactivation in photocatalytic reactions. Different approaches, such as the use of coupled SiO_2/TiO_2 catalysts [15], the addition of noble metals [16] and the sulfation of titania [17] have been assayed. In recent works, we have

* Corresponding author. Present address: Unidad de Sistemas de Concentración Solar, CIEMAT. Avda. Complutense 22, 28040 Madrid, Spain. Fax: +34 91 346 6037.
E-mail address: fernando.fresno@ciemat.es (F. Fresno).

0926-3373/$ – see front matter © 2008 Elsevier B.V. All rights reserved.
doi:10.1016/j.apcatb.2008.05.015

reported on the high photocatalytic activity for the degradation of methylcyclohexane (MCH) vapours of Sn-doped and Zr-doped TiO_2 nanosized materials [18,19], in which only TiO_2 crystalline structures (anatase–rutile and only anatase, respectively) were present and evidence of the incorporation of the guest cations into these structures was found. The use, for the same reaction, of coupled TiO_2/MO_2 (M = Sn or Zr) photocatalysts, in which both TiO_2 and MO_2 crystalline phases were present, led to reaction rates similar to or lower than those obtained with the use of the corresponding doped TiO_2 samples [19,20]. However, preliminary studies on toluene PCO showed a higher activity of a TiO_2 sample containing a segregated SnO_2 phase, compared to that of Sn-doped TiO_2 [21], and similar results were observed when comparing the activity of TiO_2/ZrO_2 and $Ti_{1-x}Zr_xO_2$ samples assayed under alike conditions [22]. These differences when changing the model pollutant led us to investigate the relation between the deactivation process and the superior activity of the TiO_2/MO_2 photocatalysts for the degradation of toluene vapours.

Thus, in this work, we compare the activity of doped $Ti_{1-x}M_xO_2$ and coupled TiO_2/MO_2 (M = Sn or Zr) catalysts for toluene PCO, paying special attention to the deactivation process and to the possible causes that lead to the higher photocatalytic activity of the coupled catalysts, which constitute by themselves very promising materials for environmental applications.

2. Experimental

2.1. Catalysts preparation and characterisation

The preparation of the photocatalysts has been detailed elsewhere [19,21]. Essentially, Sn-containing TiO_2 was obtained from the reaction between $TiCl_4$ and Ph_3SnOH in CH_2Cl_2 and calcination of the obtained powder at 723 K for 3 h. When commercial (Aldrich) Ph_3SnOH was used as received, the presence of Ph_2SnO in the starting reagent led to the formation of segregated SnO_2 in the TiO_2/SnO_2 sample, while when Ph_3SnOH was previously recrystallised, Sn-doped TiO_2 (labelled TiSn) was obtained. The Zr-doped TiO_2 sample named TiZr was obtained by the inverse microemulsion method from $ZrO(NO_3)_2$ and $Ti(O^iPr)_4$ and calcined at 773 K for 3 h, whereas the sample of ZrO_2 supported on TiO_2 (TiO_2/ZrO_2) was synthesised in a similar way by adding the previously prepared TiO_2 powder to an inverse microemulsion containing the zirconyl nitrate solution. The amounts of Sn or Zr in these samples are indicated in Table 1. Laboratory-made TiO_2 was obtained by hydrolysis of $TiCl_4$ in an inverse emulsion of water in CH_2Cl_2, followed by calcination at 723 K for 3 h. For ZrO_2 preparation, $ZrO(NO_3)_2$ was added to a microemulsion of water in *n*-heptane and the obtained powder was calcined for 3 h at 773 K. In addition, commercial SnO_2 (Probus) and the well-known P25 TiO_2 photocatalyst from Degussa were used as references.

The tin and zirconium contents were determined by total reflection X-ray fluorescence spectroscopy (TXRF), using a TXRF EXTRA-II Rich & Seifert equipment. BET surface areas were obtained from N_2 adsorption isotherms measured at 77 K in a Micromeritics 2100 apparatus. Powder X-ray diffraction (XRD) patterns were recorded on a Seifert XRD 3000P diffractometer using nickel-filtered Cu Kα radiation. The average particle size was calculated by means of the Scherrer equation from the width of the most intense reflection of each crystalline phase. Diffuse reflectance infrared Fourier transform (DRIFT) spectra were recorded on a Bruker Equinox 55 spectrometer equipped with an MCT detector operating at 77 K, accumulating 100 scans with 4 cm^{-1} resolution. A Praying Mantis© device (Harrick) was employed to register the DRIFT spectra of the sample powders. Diffuse reflectance UV–vis spectra, registered on a Shimadzu UV-2401 PC spectrometer using $BaSO_4$ as a reference, were used to estimate the band gap energy of the different samples, according to the procedure described by Serpone et al. [23].

Electron paramagnetic resonance (EPR) measurements were performed at 77 K in a Bruker ER200D instrument operating in the X-band using a double T type cavity. Aliquots of the catalyst (ca. 80 mg) were placed into a special cell made of quartz with very low iron content and provided with greaseless stopcocks. Outgassing treatments and gas adsorption were carried out by attaching the cell to a conventional vacuum manifold, which achieves pressures down to 10^{-4} N m^{-2}. The frequency of the microwave was calibrated for each experiment using a standard of diphenyl-picryl-hydrazyl (DPPH) located in the second cavity, which shows an intense symmetric signal at $g = 2.0036$. Irradiation treatments were carried out for 15 min at 77 K by placing the cell in an uncoated quartz Dewar flask filled with liquid N_2. This low operation temperature is crucial for increasing the sensitivity and stabilising labile species. For these experiments, four fluorescent lamps (Sylvania, 6WBLB-T5, 6 W, maximum intensity at 356 nm) were used as UV source. In a typical experiment, the sample was first evacuated at room temperature for 1 h, in order to obtain a hydroxylated surface free of other weakly adsorbed molecules, then dosed with small pressure of oxygen (≈10 Torr) at 77 K, evacuated for 30 min to remove the excess oxygen, which can reduce the sensitivity of the measurement to adsorbed species, and UV-irradiated for 15 min.

Table 1
Characteristics of the photocatalysts

Sample	Sn or Zr content (atom%)[a]	S_{BET} (m^2 g^{-1})	Crystalline phases	Crystal size (nm)	Indirect Band gap (eV)
TiSn	8	36	Anatase Rutile	29 6	3.0
TiZr	8	76	Anatase	10	2.9
TiO_2/SnO_2	15	41	Anatase Rutile SnO_2	26 6 5	3.0
TiO_2/ZrO_2	5	34	Anatase Tetragonal ZrO_2	14 15	3.0
TiO_2	0	47	Anatase	16	3.0
SnO_2	100	4	Rutile type	84	3.6
ZrO_2	100	73	Tetragonal ZrO_2	9	3.4
P25	0	44	Anatase Rutile	23 34	3.0

[a] Cation basis.

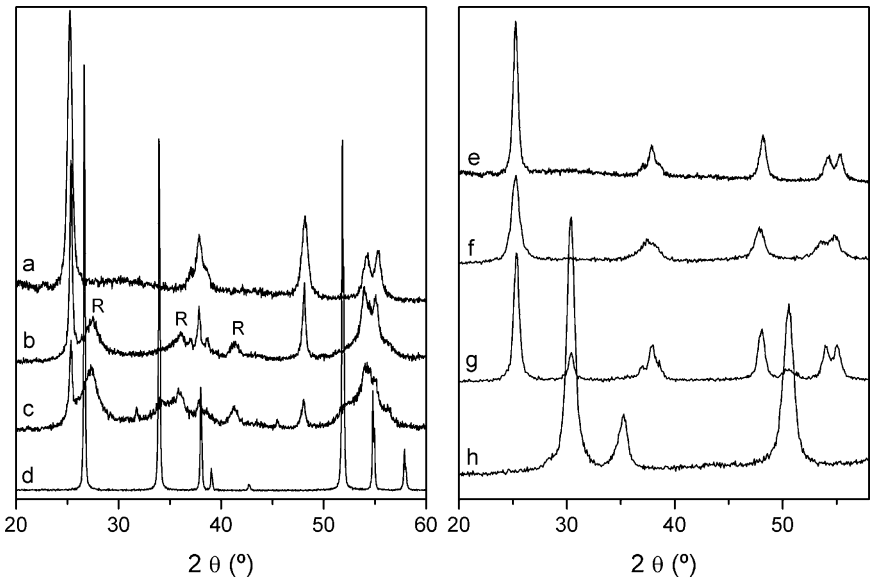

Fig. 1. XRD patterns of TiO_2 (a and e), TiSn (b), TiO_2/SnO_2 (c), SnO_2 (d), TiZr (f), TiO_2/ZrO_2 (g) and ZrO_2 (h). R: rutile.

2.2. Photocatalytic activity measurements

Toluene PCO experiments were carried out in a continuous flow annular photoreactor, constituted of two concentric Pyrex cylinders externally illuminated by four symmetrically positioned UV lamps (Sylvania, 6WBLB-T5, 6 W, maximum emission at 356 nm) [8]. A slurry of the catalyst powder in ethanol was spread on the external surface of the inner glass cylinder, and dried at room temperature to form a relatively uniform coating. The amount of catalyst (ca. 0.035–0.040 g, gravimetrically measured) and the illuminated area were the same in all the photocatalytic experiments. The reactant mixture was prepared by injecting ca. 700 ppmv of toluene (Panreac, 99%) with a syringe pump into a 100 $cm^3\ min^{-1}$ oxygen stream, controlled by a mass flow meter, that flowed through the space between the two cylinders. The water content of the reactant gas was controlled by a second syringe pump, which allowed the experiments to be performed under either humid (ca. 75% relative humidity, RH) or dry conditions (<1% RH). Before illumination, the system was equilibrated in the dark by flowing the reactant mixture. Regular analyses of the outlet gas flow were carried out by means of a Hewlett Packard GC/MS, using a HP-5 (0.25 mm × 30 m, (5% phenyl)-methylpolysiloxane) capillary column and the SIM (selected ion monitoring) mode of the detector.

2.3. Solid–liquid extractions of the used catalysts

For the analysis of the species adsorbed on the catalysts after the reactions, the powders were removed from the reactor and placed in a beaker with methanol. The mixture was stirred for several hours and the solid was separated by means of a 0.45 μm nylon syringe filter. The extract was then concentrated and analysed by GC/MS using the *scan* mode of the detector.

3. Results

3.1. Characteristics of the photocatalysts

Table 1 shows the Sn and Zr contents and the structural and morphological characteristics of the different samples, as well as their estimated band gap energies.

The doped samples (TiSn and TiZr) contain the same dopant atomic content, while their phase composition varies with the nature of the guest cation. Whereas the TiZr sample exhibits the anatase structure, equally to the laboratory-made TiO_2, the TiSn photocatalyst presents, in addition to anatase, very small rutile TiO_2 crystals, which formation is favoured by the presence of Sn^{4+} [24,25]. The presence of a segregated ZrO_2 or SnO_2 phase was detected neither in Zr- nor in Sn-doped TiO_2, as it can be observed in the XRD patterns displayed in Fig. 1. Modifications, due to the dopant cation, of anatase in the case of TiZr, and both anatase and rutile phases in the case of TiSn, have been observed from different spectroscopic techniques, and have been thoroughly reported elsewhere [19,26]. However, no evident modifications of the indirect band gaps with respect to TiO_2 were found as estimated from UV–vis spectra (see Table 1).

With regard to the coupled TiO_2/MO_2 photocatalysts, the presence of the second oxide is observed in the XRD patterns shown in Fig. 1. The TiO_2/SnO_2 sample presents wide diffraction peaks corresponding to SnO_2 with very small crystal size (see Table 1), in addition to the anatase and rutile TiO_2 phases that are also present in the doped TiSn sample. When comparing the Sn containing samples, Table 1 shows that the main difference between TiSn and TiO_2/SnO_2 is the presence of cassiterite in the latest sample, while the BET surface area and the size of both anatase and rutile crystals are quite similar. Based on the synthesis route and characterisation data, it was proposed that TiO_2/SnO_2 contains the Sn^{4+} cation both as TiO_2 dopant and as segregated SnO_2 [21]. It should be noted that the tin amount in TiSn and TiO_2/SnO_2 cannot be modulated from the preparation procedure, because it depends on the adsorption of organotin compounds on the precipitating TiO_2 particles, and the amount of Ph_2SnO in commercial Ph_3SnOH. After calcination, the former is responsible for the doping Sn atoms in both TiSn and TiO_2/SnO_2, while the latter gives rise to the SnO_2 phase in TiO_2/SnO_2 [21]. The TiO_2/ZrO_2 catalyst shows diffraction peaks corresponding to the anatase structure of TiO_2 and the tetragonal phase of ZrO_2, being the latter the only phase detected in the laboratory-made pure ZrO_2. Although the thermodynamically stable phase of ZrO_2 is monoclinic below 1200 °C, the formation of the metastable tetragonal phase is favoured in ZrO_2 crystals with size below ca. 30 nm [27]. ZrO_2 and TiO_2 crystals exhibit a similar size in the coupled

material. Whereas the presence of Zr in the anatase structure (sample TiZr) leads to an increase in the S_{BET} with respect to undoped TiO_2, related to a lower crystallite size, the sample TiO_2/ZrO_2 exhibits a slightly smaller specific surface area. As described in detail elsewhere [19], no modification in the anatase structure was observed in TiO_2/ZrO_2 with respect to pure TiO_2. Regarding the band gap energies, as obtained from the UV–vis spectra and summarized in Table 1, no evident modification with respect to either pure TiO_2 or the doped samples was found in the coupled oxides.

3.2. Photocatalytic oxidation of gaseous toluene

In the degradation of toluene over the studied photocatalysts, CO_2 was the main product detected in the gas phase. Only traces of benzaldehyde were detected in some cases at the reactor outlet, although, as it will be described later, minor amounts of less volatile intermediates accumulated on the surface of the photocatalysts during the reactions.

Fig. 2 shows the evolution of the toluene PCO reaction with irradiation time, measured as the rate of toluene removal per unit of surface area of the catalysts, obtained with the different samples under conditions of ca. 75% relative humidity. In addition, the results obtained with the TiO_2 P25 photocatalyst from Degussa, usually employed as a benchmark in photocatalysis, are displayed for comparison. The curves reveal an evident difference in the performance of the TiO_2/MO_2 photocatalysts and the doped TiSn and TiZr samples. Both the TiO_2/SnO_2 and the TiO_2/ZrO_2 catalysts give rise to a clearly superior photocatalytic activity in the steady state due to the absence of the marked deactivation process that is observed in the other photocatalysts, including the commercial P25 sample. The laboratory-made TiO_2 shows the same deactivation process and its curve is not included in Fig. 2 for the sake of clarity. SnO_2 and ZrO_2, as expected, showed no measurable activity for this photocatalytic reaction [28,29]. Thus, if the behaviour of the different samples is compared, it can be inferred that, contrarily to what it was observed in the degradation of MCH [18,19], tin- or zirconium-doping in samples TiSn and TiZr does not improve the photocatalytic activity of TiO_2 for toluene degradation, but a considerable increase, due to resistance to deactivation, is obtained when a SnO_2 or ZrO_2 phase is present.

The evolution of toluene PCO rate with irradiation time over selected catalysts in the absence of water vapour (RH < 1%) is displayed in Fig. 3. Contrarily to what it was observed when water vapour was fed into the reaction mixture, the TiO_2/MO_2 catalysts do experience a deactivation process, although in a less pronounced manner in the case of TiO_2/ZrO_2. These results indicate that the presence of water plays a key role in the beneficial effect of SnO_2 and ZrO_2 in the TiO_2/MO_2 photocatalysts that was observed in Fig. 2.

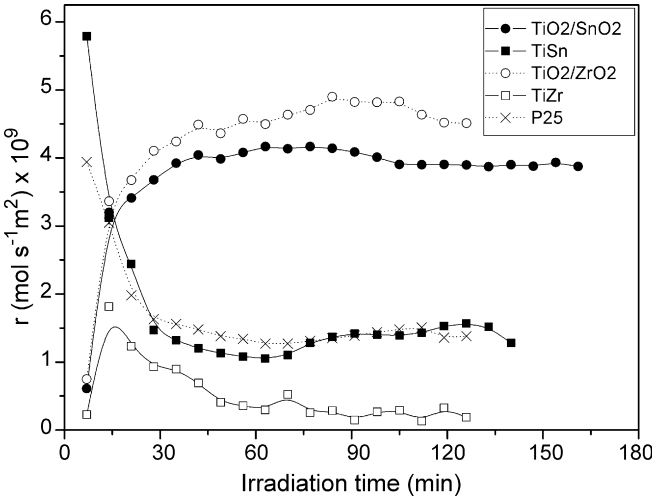

Fig. 2. Toluene photocatalytic degradation rates under humid conditions.

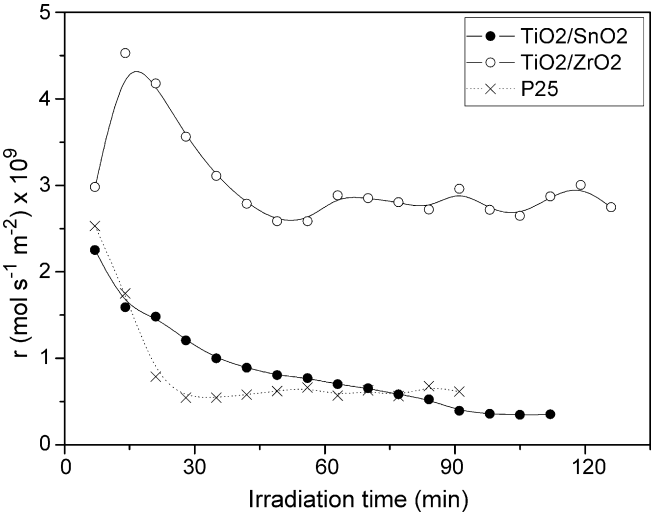

Fig. 3. Toluene photocatalytic degradation rates under dry conditions.

3.3. DRIFT spectra of fresh and used catalysts

Fig. 4 shows the DRIFT spectra of the different fresh catalysts, including that of P25, in the region where the O–H stretching vibrations appear. For TiO_2, isolated OH groups absorb around 3700 cm^{-1}, while water molecules linked by weak hydrogen bonds absorb around 3420 cm^{-1} and those linked in a more ordered arrangement, and with stronger hydrogen bonds, around 3200 cm^{-1} [30]. In the spectra shown in Fig. 4, the samples formed by TiO_2 phases (anatase or anatase–rutile mixtures: P25, TiO_2, TiSn, TiZr) display, although with different intensity, similar shapes of the wide band corresponding to the O–H stretching

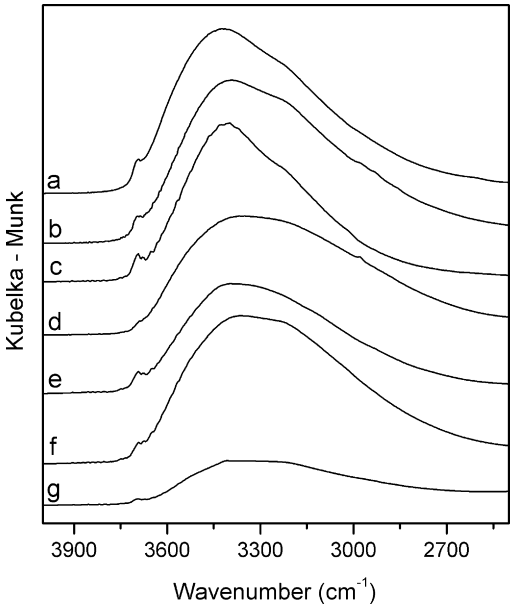

Fig. 4. DRIFT spectra of fresh samples: (a) ZrO_2, (b) TiO_2/ZrO_2, (c) TiO_2/SnO_2, (d) TiZr, (e) TiSn, (f) TiO_2 and (g) P25.

vibrations of water molecules. However, the spectra of the TiO_2/MO_2 samples present a different shape of this band (especially marked in TiO_2/SnO_2), with a higher contribution of water molecules linked by weak hydrogen bonds (band around 3420 cm^{-1}). These water molecules should be more mobile and accessible for participation in the photocatalytic reaction. In addition, the spectrum of the laboratory-made ZrO_2 also shows a higher contribution of the band appearing close to 3420 cm^{-1}, as it can be observed in Fig. 4. On the other hand, the commercial SnO_2 sample used in this study has a high crystal size and a low surface area (see Table 1) and, as a consequence, its DRIFT spectrum shows a very low amount of adsorbed water and it has not been included in Fig. 4. In contrast, the spectra of SnO_2 samples with very small crystal size (as in the case of the SnO_2 phase present in the TiO_2/SnO_2 sample, see Table 1), reported by Chen and Gao, also show, in the broad band of adsorbed water, a considerably higher contribution of the band corresponding to water molecules linked by weak hydrogen bonds [31]. Thus, the differences in the adsorbed water observed in the DRIFT spectra between the SnO_2 or ZrO_2-containing catalysts and the rest of samples may be ascribed to the presence of the segregated Sn or Zr oxide.

Fig. 5 shows the DRIFT spectra in the 1200–1800 cm^{-1} region of samples that were deactivated (TiO_2 and TiZr, left part of the figure) and others that were not (TiO_2/SnO_2 and TiO_2/ZrO_2, right part) after being used for toluene PCO under humid conditions. The contribution of the fresh photocatalyst has been subtracted from the spectra of the used samples, so that only the bands corresponding to species formed during the reaction are visible. In the case of TiO_2 and TiZr, several bands corresponding to different adsorbed reaction intermediates are observed, and both spectra contain essentially the same bands, although with different relative intensities. The bands at 1411 and 1513 cm^{-1} can be assigned to the ν_s and ν_{as} stretching vibrations, respectively, of COO^- groups anchored to the TiO_2 surface [15,16,32–34], although the former can also present contributions from δ(HCH) vibrations [35]. The aromatic ring vibrations are reflected in the bands at 1604 and 1448 cm^{-1} [15,16,35–37]. The bands at 1688 and 1713 cm^{-1} are assigned to C=O stretching vibrations of carbonyl compounds, being the former very close to that reported in the literature for benzaldehyde [15,16,32,37]. Thus, the DRIFT spectra of used TiO_2 and TiZr reveal the presence of aromatic, carbonylic and carboxylic compounds. Actually, the spectra contain the bands that have been reported for benzoic acid adsorbed on the TiO_2 surface as benzoate [32], as well as for hemiacetalic groups, which are carboxylate precursors and are formed by nucleophilic attack of $^{\bullet}OH$ radicals to carbonyl groups [38]. In good accordance with the DRIFT spectrum, in the analysis of a solid–liquid extract of the species adsorbed on the used TiO_2 catalyst, the main species found was benzoic acid, and peaks corresponding to benzyl alcohol and benzaldehyde, all of them formed by oxidation of the methyl group of toluene, were also observed by GC/MS analysis. Other detected species were 2-hydroxybenzaldehyde and, as the only intermediate coming from the cleavage of the aromatic ring, acetic acid. In addition, the detected methyl benzoate was probably formed by esterification of benzoic acid with the methanol used as solvent.

As far as the coupled photocatalysts are concerned, the spectra shown in Fig. 5 display considerable differences with those of the deactivated catalysts. In the region between 1200 and 1800 cm^{-1}, both TiO_2/SnO_2 and TiO_2/ZrO_2 show negative bands which may arise from the elimination of carbonaceous residues remaining on the catalyst after calcination. Apart from that, the main differences from the spectra of TiO_2 and TiZr are, on the one hand, the absence of the peak assigned to the COO^- antisymmetric stretching vibration, which suggests a lower amount of carboxylate species, and, on the other hand, the nearly absence of the aromatic ring vibrations observed from the bands at 1604 and 1448, the first of which is only observable as a shoulder in the TiO_2/SnO_2 spectrum. Fig. 6 shows the DRIFT spectra of the TiO_2/SnO_2 sample after being used in toluene PCO under humid and dry conditions, the latter case leading to deactivation of the catalyst. As it can be observed, in both cases similar bands appear, although under dry conditions the contribution of the aromatic ring vibrations is considerably larger, as indicated by the higher intensity of the bands at 1604 and 3067 cm^{-1}, the latter corresponding to aromatic C–H stretching vibrations. In addition, a larger contribution of C(sp^3)–H stretching is observed, as indicated by the bands appearing below 3000 cm^{-1}. On the other hand, the catalyst used under humid conditions shows an expected lower loss of surface water and hydroxyl groups than that used in the absence of water vapour.

In addition to DRIFT results, in the analysis of the extract of the TiO_2/SnO_2 catalyst used under humid conditions only traces of phenol were detected, while in the case of the catalyst used under dry conditions, deactivation was accompanied by the detection of mainly benzoic acid, benzaldehyde and benzyl alcohol in the

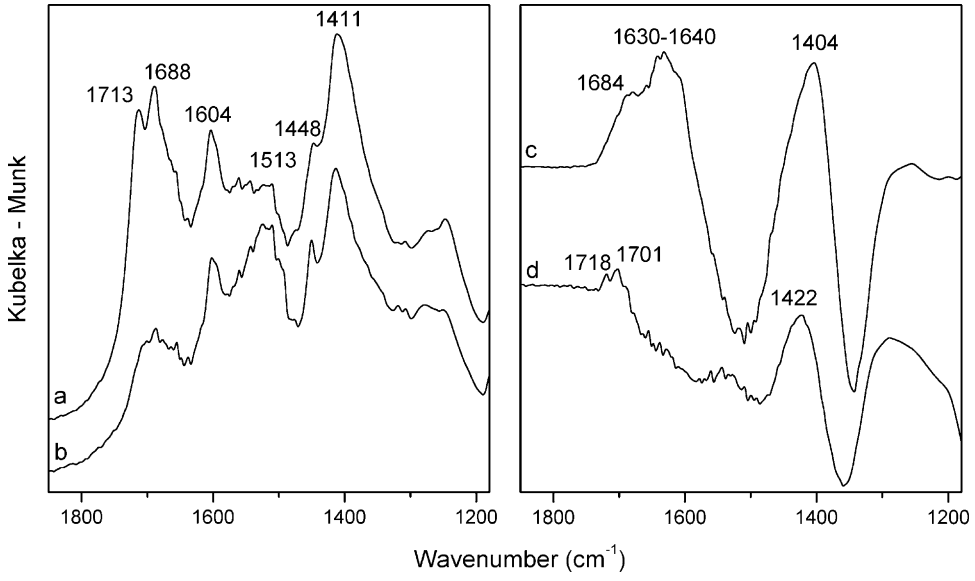

Fig. 5. DRIFT spectra of catalysts used in toluene PCO: (a) TiO_2, (b) TiZr, (c) TiO_2/SnO_2 and (d) TiO_2/ZrO_2.

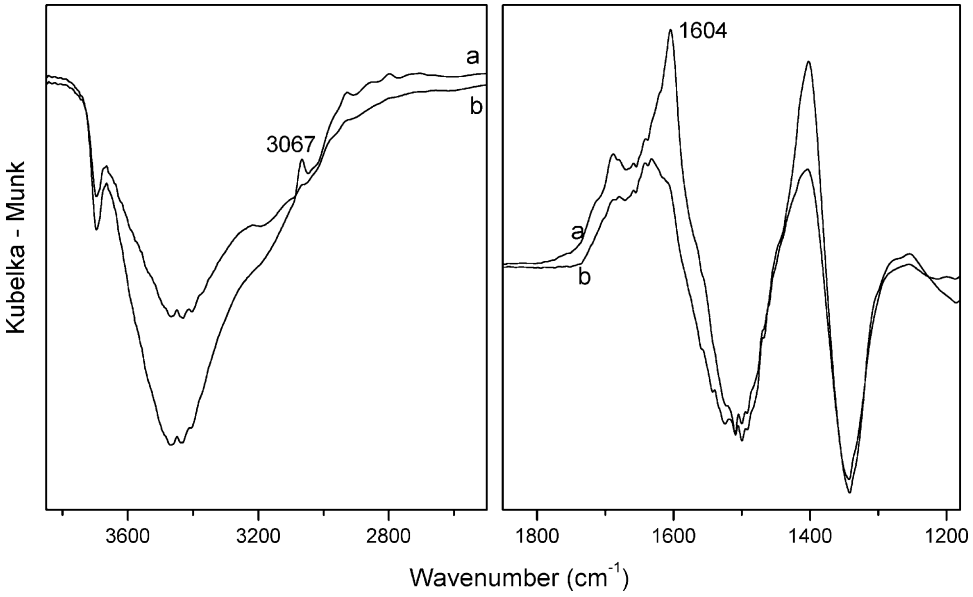

Fig. 6. DRIFT spectra of the TiO_2/SnO_2 photocatalyst used in toluene PCO under dry (a) and humid (b) conditions.

extract, similarly to what was found in the case of TiO_2. Moreover, the TiO_2/SnO_2 and TiO_2/ZrO_2 catalysts do not present, after the reaction, the yellowish colour that generally appears in deactivated TiO_2 photocatalysts and is probably related to the presence of adsorbed intermediates and/or carbon deposits [13,32].

3.4. EPR study of the photocatalysts–O_2 interaction under UV irradiation

Fig. 7 displays the EPR spectra at 77 K recorded after UV-irradiation of the photocatalysts in the presence of O_2. The spectrum corresponding to TiO_2 is comparable to those previously obtained for this material under similar treatments [39,40], and it is constituted by at least two overlapping signals at $g > g_e$ (g-factor of the free electron; $g_e = 2.0023$) related to oxygenated radicals, and a sharp axial signal with $g_\perp = 1.990$ and $g_{||} = 1.961$. This last feature can be assigned to Ti^{3+} centres in the anatase lattice generated by photoelectron capture [39,40]. Signals at lower field can be isolated by computer simulation and are basically constituted by Ti^{4+}–$O^{\bullet-}$ (components at $g_1 = 2.024$, $g_2 = 2.013$ and $g_3 = 2003$), formed by photogenerated holes trapped by O^{2-} ions, and Ti^{4+}–$O_2H^{\bullet}$ (hydroperoxy) contributions (components at $g_1 = 2.032$, $g_2 = 2.009$ and $g_3 = 2.003$), originated from the protonation of $O_2^{\bullet-}$ (superoxide) radicals [39,40]. In addition, the relatively high linewidth of the lower field component suggests that the existence of a low amount of Ti^{4+}–$O_2^{\bullet-}$ radicals (components at $g_1 = 2.024$, $g_2 = 2.009$ and $g_3 = 2.003$) cannot be discarded [40]. The spectrum obtained for the sample TiO_2/ZrO_2 is very similar to that of TiO_2, although the component at $g = 2.032$ is better resolved in this case, indicating that a higher proportion of $O_2H^{\bullet}$ species is produced on this sample. This observation is not unexpected considering that the increment in the weakly H-bonded adsorbed water observed in the IR spectra for sample TiO_2/ZrO_2, in comparison with the unmodified TiO_2 (see Fig. 4), can supply the protons for the formation of hydroperoxy radicals. On the other hand, the intensity of Ti^{3+} signal also increases notably, but, in contrast, no indication of the formation of Zr^{3+} centres is found. Those species are neither detected in the case of the TiZr sample, although the Ti^{3+} species formed by UV-irradiation in this material present slightly different parameters: $g_\perp = 1.990$ and $g_{||} = 1.958$. This variation could be related to the modification of the environment of the Ti^{3+} sites by zirconium incorporation. Similarly, the spectrum of the TiZr sample is dominated at $g > g_e$ by a signal with $g_1 = 2.035$, $g_2 = 2.009$ and $g_3 = 2003$, which could correspond either to Ti^{4+}–$O_2H^{\bullet}$ species in a slightly different environment than in the case of TiO_2/ZrO_2, or, alternatively, to Zr^{4+}–$O_2^{\bullet-}$ radicals. Several studies have shown that superoxide species attached to zirconium cations present orthorhombic signals with $g_1 = 2.037$–2.033, $g_2 = 2.010$–2009 and $g_3 = 2.004$–2.002 [41–43]. Therefore, although a more detailed investigation

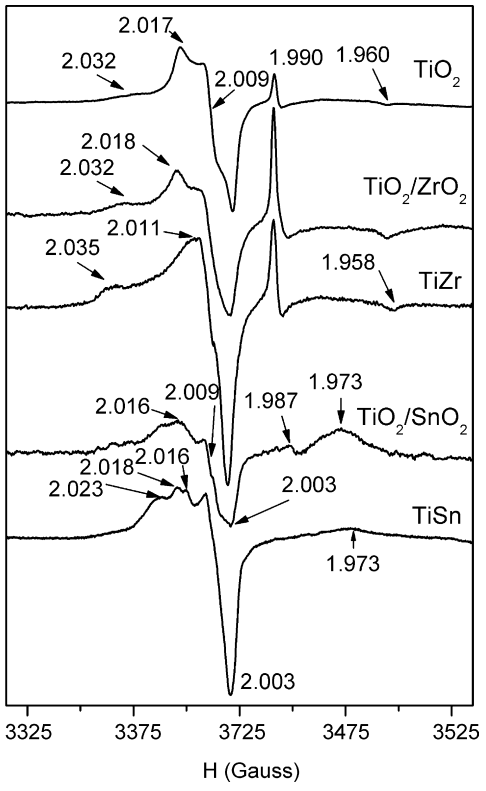

Fig. 7. EPR spectra at 77 K of the different photocatalysts UV-irradiated for 15 min in the presence of adsorbed oxygen.

Table 2
EPR parameters of the radicals detected on the different photocatalysts upon UV-irradiation in the presence of adsorbed oxygen at 77 K

Radical	EPR parameters	Photocatatalysts on which these species are detected
$Ti^{4+}–O^{\bullet-}$	$g_1 = 2.024$, $g_2 = 2.013$, $g_3 = 2.003$	TiO_2, TiZr, TiO_2/ZrO_2, TiSn
	$g_1 = 2.028$, $g_2 = 2.017$, $g_3 = 2.003$	TiSn
$Ti^{4+}–O_2^{\bullet-}$	$g_1 = 2.025$, $g_2 = 2.009$, $g_3 = 2.003$	TiO_2, TiO_2/ZrO_2
$Zr^{4+}–O_2^{\bullet-}$ [a]	$g_1 = 2.035$, $g_2 = 2.009$, $g_3 = 2.003$	TiZr
$Ti^{4+}–O_2H^{\bullet}$	$g_1 = 2.032$, $g_2 = 2.009$, $g_3 = 2.003$	TiO_2, TiO_2/ZrO_2
Ti^{3+} centres in anatase	$g_\perp = 1.990$ and $g_{\|} = 1.961$	TiO_2, TiZr
Ti^{3+} centres in anatase	$g_\perp = 1.990$ and $g_{\|} = 1.958$	TiO_2/ZrO_2
Ti^{3+} centres in rutile	$g_\perp = 1.973$	TiSn, TiO_2/SnO_2

[a] Tentative assignment.

would be necessary to ascertain this point, considering the composition and the low hydration degree of the TiZr sample, it seems plausible to ascribe the oxygenated radicals photogenerated on this materials to the $Zr^{4+}–O_2^{\bullet-}$ moiety. Accepting these assignments (see Table 2), remarkable differences in the fate of photogenerated electrons are envisaged for samples TiZr and TiO_2/ZrO_2. In this way, supported ZrO_2 modify the photoexcitation of TiO_2 quantitatively by increasing the ratio $Ti^{3+}/Ti^{4+}–O_2H^{\bullet}$, while the incorporation of Zr into the anatase lattice causes modification of the trapping centres.

The EPR spectrum of the TiO_2/SnO_2 sample recorded upon irradiation in oxygen is more complex than the other spectra shown in Fig. 7 because of the different phases present in this material (see Table 1). In particular, the spectrum differs from those of the Zr-containing samples in several aspects: the intensity at $g < g_e$ is significantly lower and the sharp peaks characteristic of Ti^{3+} centres in anatase are absent. On the other hand, a new relatively broad signal at $g = 1.973$ can be observed for this mixed photocatalyst. Signals with $g_\perp = 1.975$ have been observed upon irradiation of TiO_2 samples containing rutile crystallites, and they have been ascribed to Ti^{3+} centres located in this phase [44]. In the case of TiO_2/SnO_2 sample, this assignment seems to be likely, considering the high proportion of rutile detected by XRD in this sample, and the small shift of the signal could be related to the modification of the electron traps by Sn^{4+} incorporation, bearing in mind that, as it was mentioned earlier, this sample contains Sn^{4+} both as a dopant cation in TiO_2 and as segregated SnO_2. The $g_{\|}$ component of this signal should appear at ca. 1.940, but it is not observed due to its lower intensity. Similarly, the weak feature at 1.987 could be related to the $g_\perp$ parameter of a small amount of modified Ti^{3+} sites in anatase matrix. Finally, the spectrum of the TiO_2/SnO_2 sample at $g > g_e$ basically comprises a signal of $Ti^{4+}–O^{\bullet-}$ akin to that detected in pure TiO_2. Besides, the very weak component at $g = 2.009$ suggests that a small amount of $Ti^{4+}–O_2^{\bullet-}$ radicals is also formed on this sample. In spite of this, a comparison with the results obtained for the TiO_2/ZrO_2 sample shows that transference of photoelectrons to O_2 is relatively hindered for the TiO_2/SnO_2 photocatalyst. This observation may be due to the migration of photoproduced electrons to the SnO_2 phase [25], which implies certain loss of energy that can hamper subsequent electron trapping by acceptor molecules, particularly at the temperature of the EPR measurements (77 K). On the other hand, EPR results reveal that electron capture takes place mainly on sites of the rutile phase, and consequently these data are compatible with electron transference from anatase $Ti_{1-x}Sn_xO_2$ to SnO_2, rather than from rutile $Ti_{1-x}Sn_xO_2$ to SnO_2.

At high field, the EPR spectrum of TiSn sample shows only a very weak signal at $g = 1.973$, which very likely corresponds to a low concentration of Ti^{3+} centres in a rutile matrix. In contrast, the spectrum of this sample presents a significant intensity for $g > g_e$, which can be related to different types of oxygenated radicals. Although identification of each contribution in this complex spectrum is difficult, the following parameters can be tentatively estimated for these overlapping signals: A with $g_1 = 2.028$, $g_2 = 2.017$ and $g_3 = 2.003$; B with $g_1 = 2.024$, $g_2 = 2.014$ and $g_3 = 2.003$; and C with $g_1 = 2.025$, $g_2 = 2.009$ and $g_3 = 2.003$. The first two signals can be ascribed to $Ti^{4+}–O^{\bullet-}$ radicals located either on the surface (signal A) or in the bulk on the solid (signal B) [40], as it has been observed in the other samples studied in this work. As detected in other samples, signal C can be assigned to superoxide radicals bound to titanium centres. However, no features attributable to the formation $Sn^{4+}–O_2^{\bullet-}$ species ($g_1 = 2.023$, $g_2 = 2.006$ and $g_3 = 2.003$) [45] were detected in the spectrum of TiSn sample. A comparison of these results with those obtained for the sample TiZr suggests that localized electron traps (i.e. Ti^{3+}) are rather scarce for the sample containing Sn. Higher photoelectron delocalization and/or a higher rate of transference to the surface or between phases could account for these observations.

4. Discussion

In order to discuss the origin of the superior photocatalytic activity of the coupled oxides for toluene PCO, it seems advisable to distinguish between the mechanisms that make the materials present a high intrinsic activity, which may be represented by the performance in methylcyclohexane (MCH) PCO, and those leading to the resistance to deactivation, which finally result in a higher activity for the degradation of toluene.

In the case of TiZr and other related samples, an increased concentration of strong acid OH groups was found with respect to TiO_2, which was associated to a high photocatalytic activity for the degradation of MCH vapours [19]. This increased surface acidity has been related to the formation of heterometallic Ti–O–Zr assemblies [19,46,47]. In the same way, the TiO_2/ZrO_2 catalyst exhibited lower acidity than the doped samples and gave rise to lower MCH conversions [19]. However, in the case of the toluene PCO reported here, this correlation between acidity and photoactivity does not seem to exist. On the one hand, despite the lower surface acidity of TiO_2/ZrO_2 [19], it presents a resistance to deactivation not observed in the Zr-doped sample, as shown in Fig. 2. On the other hand, deactivation of TiZr in toluene PCO may be related to the presence of a higher number of strong acid sites (acidic surface hydroxyls) which, although they favour charge separation and consequently seem to play a key role in the photodegradation of MCH [19], would be deactivated more easily than others, since these surface hydroxyl groups are strong adsorption sites [46]. However, TiO_2/ZrO_2, presenting higher surface acidity than TiO_2, shows a remarkably better performance for toluene PCO. These comparisons suggest that other factors different from surface acidity are influencing the behaviour of TiO_2/ZrO_2 in this reaction. In the literature, although the combination of TiO_2 and ZrO_2 in photocatalysis is generally related to the use of mixed oxides [46–50], the coupling of both components as separate crystalline phases has also been reported.

Colón et al. observed an improvement in the photocatalytic activity of calcined Degussa P25 with the addition of ZrO_2, which they ascribed mainly to the stabilization of the anatase structure and the modification of adsorptive properties [51].

The improvement in the photocatalytic activity of TiO_2 by coupling with SnO_2 has been reported in several works [28,52–60]. In all of them, this improvement is ascribed to a decrease in the electron-hole recombination rate due to the charge separation occurring through the interface between both semiconductors. This charge separation has been also observed in anatase–rutile composite photocatalysts [61], and it was proposed as one of the factors, in addition to electronic effects caused by Sn incorporation, that led to the high photocatalytic activity of TiSn and related samples for the elimination of MCH vapours [18]. In addition, the incorporation of Sn^{4+} ions to the TiO_2 lattice, similarly to other oxidic systems, has been found to increase the surface acidity of the parent oxide [62], which may, as mentioned earlier, increase the photocatalytic activity but also favour deactivation. These factors also exist in the TiO_2/SnO_2 sample and consequently its activity for MCH degradation is similar to that of the Sn-doped sample and higher than that of TiO_2 [20]. However, the doped anatase/rutile sample TiSn does experience deactivation during the photocatalytic oxidation of toluene, differently to TiO_2/SnO_2. Thus, charge separation in different crystallographic phases and tin-doping cannot be the only factors leading to the good performance of the TiO_2/SnO_2 catalyst in toluene PCO. Regarding water adsorption properties of coupled photocatalysts, the positive effect of SnO_2 has been also ascribed to a higher hydrophilicity of TiO_2/SnO_2 photocatalysts compared to TiO_2 [59], and Kanai et al. reported a correlation between the hydrophilic/hydrophobic conversion rates of TiO_2/SnO_2 stacks and their photocatalytic efficiencies for the degradation of gaseous isopropanol [63,64]. In addition, Cao et al. observed a higher water adsorption capacity in nanosized SnO_2 than in TiO_2 [65].

From the obtained results, it appears that different mechanisms, depending on the dopant cation, govern the high photocatalytic activity of the doped samples for MCH elimination, in which deactivation is not important. On the other hand, a similar behaviour is found for both TiO_2/SnO_2 and TiO_2/ZrO_2 with respect to deactivation in the case of toluene PCO. As it was mentioned earlier, surface water seems to play a key role in the activity of the TiO_2/MO_2 photocatalysts. In this respect, in the case of coupled catalysts, a correlation between the surface water and the high photocatalytic activity seems to exist. In the case of toluene PCO, as observed in the DRIFT spectra shown in Fig. 4, more accessible adsorbed water, due to the presence of the second oxide, may increase the capacity of TiO_2 for the removal of the adsorbed intermediates that cause the deactivation of the photocatalysts. The relation between adsorbed intermediates and deactivation is observed in the comparison of the DRIFT spectra and the solid–liquid extractions of deactivated and non-deactivated catalysts after their use in the toluene PCO reaction. In this respect, it is observed that both TiO_2/ZrO_2 and TiO_2/SnO_2 photocatalysts suffer a lower accumulation of intermediates after the toluene PCO reaction under humid conditions, in which case they do not present the deactivation observed in the rest of assayed samples. In other words, the water adsorption characteristics of the coupled photocatalysts favours the mineralisation of toluene against the formation of partial oxidation products, some of which can remain adsorbed on the catalyst surface. The main differences between the surface of these catalysts and the deactivated ones are a smaller accumulation of non-volatile carboxylates and aromatic species, the latter appearing to be more influential, as they are clearly observed in the spectrum of TiO_2/SnO_2 under the dry conditions that lead to catalyst deactivation. The stability of the aromatic ring appears to be one of the factors leading to the deactivation process of some of the studied catalysts during toluene PCO. In fact, the benzylperoxy radical, $C_6H_5–CH_2OO^{\bullet}$, which results from the highly stable benzyl radical, has been detected by EPR spectroscopy in the initial stages of toluene PCO [66].

EPR results support the idea that, in the case of the TiO_2/ZrO_2 photocatalyst, a greater interaction with surface water is occurring, which leads to the observation of a higher amount of $O_2H^{\bullet}$ radicals. Also in agreement with the previous discussion, the differences between TiO_2 and TiZr samples are mainly due to structural modifications that influence electron trapping sites. In this way, transference of photoelectrons seems to take place preferentially on Zr centres for the doped sample. However, in the case of TiO_2/SnO_2, the EPR spectrum does not reveal information about the influence of surface water given the low intensity and the complexity of the spectrum in the region at $g > g_e$. On the other hand, in both doped and coupled Sn-containing samples, an electron transfer between phases is suggested. These factors may justify the similar behaviour of TiSn and TiO_2/SnO_2 in MCH PCO, but do not explain the difference in their performance for toluene degradation. Photoelectron migration is neither possible in TiZr, which contains only the anatase phase, nor in TiO_2/ZrO_2, in which such transfer is not permitted since the conduction band energy of tetragonal ZrO_2 is above that of anatase [67,68]. Nevertheless, in the case of TiZr the heteroatom participates in electron trapping sites leading to the formation of $Zr^{4+}–O_2^{\bullet-}$ species, and this may influence the intrinsic photoactivity of this material.

5. Conclusions

The photocatalytic degradation of toluene over doped $Ti_{1-x}M_xO_2$, formed only by TiO_2 (anatase or anatase–rutile mixtures) phases, and coupled TiO_2/MO_2 (M: Sn, Zr) has been studied. The coupled photocatalysts give rise to a higher degradation rate due to the absence of the deactivation process that occurs with the doped samples and with the TiO_2 reference. The lack of deactivation is linked to a lower accumulation of adsorbed intermediates during the photocatalytic reaction for the coupled catalysts, with respect to the deactivated samples, as shown by DRIFT spectra and solid–liquid extraction of the used catalysts. DRIFT spectra of the fresh catalysts reveal a higher contribution of adsorbed water molecules linked by weak hydrogen bonds in the coupled samples. EPR spectra of the samples irradiated in the presence of adsorbed O_2 reveal a higher contribution of $O_2H^{\bullet}$ radicals in TiO_2/ZrO_2 with respect to TiO_2, in agreement with the DRIFT results. Unfortunately, no conclusive results are observed in TiO_2/SnO_2 in this respect. As far as the doped TiO_2 samples are concerned, EPR spectra reveal modifications in the electron trapping sites with both dopant cations and, in the case of the $Ti_{1-x}Sn_xO_2$ catalyst, an electron transfer from anatase to rutile, which is also present in TiO_2/SnO_2. The obtained results lead us to conclude that, while structural and electronic modifications, due to the guest cations, are responsible for the high activity of doped samples observed in previous studies for a reaction not causing catalyst deactivation (methylcyclohexane PCO), the resistance to deactivation of the coupled photocatalysts observed in toluene PCO is mainly due to more accessible adsorbed water, due to the presence of the second oxide, that gives rise to a higher capacity for the removal of adsorbed reaction intermediates.

Acknowledgements

This work has received financial support from the Spanish *Ministerio de Educación y Ciencia* (MEC), through the project

CTQ2007-60480. F.F. and M.D.H.A. want to thank MEC and the *Comunidad de Madrid*, respectively, for the award of their doctoral grants.

References

[1] A.M. Linsebigler, G. Lu, J.T. Yates, Chem. Rev. 95 (1995) 735.
[2] J.M. Herrmann, Catal. Today 53 (1999) 115.
[3] O. Carp, C.L. Huisman, A. Reller, Prog. Sol. State Chem. 32 (2004) 33.
[4] Y. Luo, D.F. Ollis, J. Catal. 163 (1996) 1.
[5] O. d'Hennezel, P. Pichat, D.F. Ollis, J. Photochem. Photobiol. A: Chem. 118 (1998) 197.
[6] M. Bluont, J.L. Falconer, Appl. Catal. B: Environ. 39 (2002) 39.
[7] V. Augugliaro, S. Coluccia, V. Loddo, L. Marchese, G. Martra, L. Palmisano, M. Schiavello, Appl. Catal. B: Environ. 20 (1999) 15.
[8] A.J. Maira, K.L. Yeung, J. Soria, J.M. Coronado, C. Belver, C.Y. Lee, V. Augugliaro, Appl. Catal. B: Environ. 29 (2001) 327.
[9] X. Fu, W. Zeltner, M.A. Anderson, Appl. Catal. B: Environ. 6 (1995) 209.
[10] M. Lewandowski, D.F. Ollis, Appl. Catal. B: Environ. 43 (2003) 309.
[11] M.M. Ameen, G.B. Raupp, J. Catal. 184 (1999) 112.
[12] M. Lewandowski, D.F. Ollis, Appl. Catal. B: Environ. 45 (2003) 223.
[13] H. Einaga, S. Futamura, T. Ibusuki, Appl. Catal. B: Environ. 38 (2002) 215.
[14] M. Addamo, V. Augugliaro, S. Coluccia, A. Di Paola, E. García-López, V. Loddo, G. Marci, G. Martra, L. Palmisano, Int. J. Photoenergy (2006) 1–2.
[15] R. Méndez-Román, N. Cardona-Martínez, Catal. Today 40 (1998) 353.
[16] C. Belver, M.J. López-Muñoz, J.M. Coronado, J. Soria, Appl. Catal. B: Environ. 46 (2003) 497.
[17] E. Barraud, F. Bosc, D. Edwards, N. Keller, V. Keller, J. Catal. 235 (2005) 318.
[18] F. Fresno, J.M. Coronado, D. Tudela, J. Soria, Appl. Catal. B: Environ. 55 (2005) 159.
[19] M.D. Hernández-Alonso, J.M. Coronado, B. Bachiller-Baeza, M. Fernández-García, J. Soria, Chem. Mater. 19 (2007) 4283.
[20] F. Fresno, Ph.D. Thesis, Universidad Autónoma de Madrid, 2006.
[21] F. Fresno, D. Tudela, A.J. Maira, F. Rivera, J.M. Coronado, J. Soria, Appl. Organomet. Chem. 20 (2006) 220.
[22] M.D. Hernández-Alonso, Ph.D. Thesis, Universidad Autónoma de Madrid, 2006.
[23] N. Serpone, D. Lawless, R. Khairutdinov, J. Phys. Chem. 99 (1995) 16646.
[24] K.-N.P. Kumar, K. Keizer, A.J. Burggraaf, T. Okubo, H. Nagamoto, J. Mater. Chem. 3 (1993) 923.
[25] D. Tudela, F. Fresno, J.M. Coronado, in: W. Chen (Ed.), Doped Nanomaterials and Nanodevices, American Scientific Publishers, Los Angeles, 2008, in press.
[26] F. Fresno, D. Tudela, J.M. Coronado, M. Fernández-García, A.B. Hungría, J. Soria, Phys. Chem. Chem. Phys. 8 (2006) 2421.
[27] M. Fernández-García, A. Martínez-Arias, J.C. Hanson, J.A. Rodríguez, Chem. Rev. 104 (2004) 4063.
[28] K. Vinodgopal, I. Bedja, P.V. Kamat, Chem. Mater. 8 (1996) 2180.
[29] J.A. Navío, G. Colón, J.M. Herrmann, J. Photochem. Photobiol. A: Chem. 108 (1997) 179.
[30] T. Bezrodna, G. Puchovska, V. Shymanovska, J. Baran, H. Ratajczak, J. Mol. Struct. 700 (2004) 175.
[31] D. Chen, L. Gao, J. Colloid Interface Sci. 279 (2004) 137.
[32] L. Cao, Z. Gao, S.L. Suib, T.N. Obee, S.O. Hay, J.D. Freihaut, J. Catal. 196 (2000) 253.
[33] J.M. Coronado, S. Kataoka, I. Tejedor-Tejedor, M.A. Anderson, J. Catal. 219 (2003) 219.
[34] M. Sanati, A. Andersson, J. Mol. Catal. 81 (1993) 51.
[35] E. Pretsch, P. Bühlmann, C. Affolter, Structure Determination of Organic Compounds. Tables of Spectral Data, third ed., Springer-Verlag, Berlin, 2000.
[36] M. Nagao, Y. Suda, Langmuir 5 (1989) 42.
[37] A.J. Maira, J.M. Coronado, V. Augugliaro, K.L. Yeung, J.C. Conesa, J. Soria, J. Catal. 202 (2001) 413.
[38] G. Marci, M. Addamo, V. Augugliaro, S. Coluccia, E. García López, V. Loddo, G. Martra, L. Palmisano, M. Schiavello, J. Photochem. Photobiol. A: Chem. 160 (2003) 105.
[39] T. Berger, M. Sterrer, O. Diwald, E. Knozinger, D. Panayotov, T.L. Thompson, J.T. Yates, J. Phys. Chem. B 109 (2005) 6061.
[40] J.M. Coronado, A.J. Maira, J.C. Conesa, K.L. Yeung, V. Augugliaro, J. Soria Langmuir 17 (2001) 5368.
[41] E. Giamello, M. Volante, B. Fubini, F. Geobaldo, C. Morterra, Mater. Chem. Phys. 29 (1991) 379.
[42] V. Ramaswamy, B. Tripathi, D. Srinivas, A.V. Ramaswamy, R. Cattaneo, R. Prins, J. Catal. 200 (2001) 250.
[43] A. Martínez-Arias, M. Fernández-García, A.B. Hungría, J.C. Conesa, J. Soria, J. Alloy Compd. 323 (2001) 605.
[44] D.C. Hurum, A.G. Agrios, K.A. Gray, T. Rajh, M.C. Thurnauer, J. Phys. Chem. B 107 (2003) 4545.
[45] F. Morazzoni, C. Canevali, N. Chiodini, C. Mari, R. Ruffo, R. Scotti, L. Armelao, E. Tondello, L.E. Depero, E. Bontempi, Chem. Mater. 13 (2001) 4355.
[46] X. Fu, L.A. Clark, Q. Yang, M.A. Anderson, Environ. Sci. Technol. 30 (1996) 647.
[47] D. Das, H.K. Mishra, K.M. Parida, A.K. Dalai, J. Mol. Catal. A 189 (2002) 271.
[48] J.H. Shattka, D.G. Shchuskin, J. Jia, M.A. Antonietti, R.A. Caruso, Chem. Mater. 14 (2002) 5103.
[49] A. Kitiyanan, S. Ngamsinlapasathian, S. Pavasupree, S. Yoshikawa, J. Solid State Chem. 178 (2005) 1044.
[50] Y.M. Wang, S.W. Liu, M.K. Lü, S.F. Wang, F. Gu, X.Z. Gai, X.P. Cui, J. Pan, J. Mol. Catal. A: Chem. 215 (2004) 137.
[51] G. Colón, M.C. Hidalgo, J.A. Navío, Appl. Catal. A: Gen. 231 (2002) 185.
[52] H. Tada, A. Hattori, Y. Tokihisa, K. Imai, N. Toghe, S. Ito, J. Phys. Chem. B 104 (2000) 4585.
[53] K. Vinodgopal, P.V. Kamat, Environ. Sci. Technol. 29 (1995) 841.
[54] I. Bedja, P.V. Kamat, J. Phys. Chem. 99 (1995) 9182.
[55] A. Hattori, Y. Tokihisa, H. Tada, S. Ito, J. Electrochem. Soc. 147 (2000) 2279.
[56] T. Kawahara, Y. Konishi, H. Tada, N. Toghe, S. Ito, Langmuir 17 (2001) 7442.
[57] Y. Cao, X. Zhang, W. Yang, H. Du, Y. Bai, T. Li, J. Yao, Chem. Mater. 12 (2000) 3445.
[58] L. Shi, C. Li, H. Gu, D. Fang, Mater. Chem. Phys. 62 (2000) 62.
[59] Q. Liu, X. Wu, B. Wang, Q. Liu, Mater. Res. Bull. 37 (2002) 2255.
[60] J. Shang, W. Yao, Y. Zhu, N. Wu, Appl. Catal. A: Gen. 257 (2004) 25.
[61] T. Kawahara, Y. Konishi, H. Tada, N. Tohge, J. Nishii, S. Ito, Angew. Chem. Int. Ed. 41 (2002) 2811.
[62] K. Shibata, T. Kiyoura, J. Kitagawa, T. Sumiyoshi, K. Tanabe, Bull. Chem. Soc. Jpn. 46 (1973) 2985.
[63] N. Kanai, T. Nuida, K. Ueta, K. Hashimoto, T. Watanabe, H. Ohsaki, Vacuum 74 (2004) 723.
[64] H. Ohsaki, N. Kanai, Y. Fukunaga, M. Suzuki, T. Watanabe, K. Hashimoto, Thin Solid Films 502 (2006) 138.
[65] L. Cao, F.-J. Spiess, A. Huang, S.L. Suib, T.N. Obee, S.O. Hay, J.D. Freihaut, J. Phys. Chem. B 103 (1999) 2912.
[66] J.M. Coronado, J. Soria, Catal. Today 123 (2007) 37.
[67] R. Puthenkovilakam, J.P. Chang, Appl. Phys. Lett. 84 (2004) 1353.
[68] D.A. Schmidt, T. Ohta, C.-Y. Lu, A.A. Bostwick, Q. Yu, E. Rotenberg, F.S. Ohuchi, M.A. Olmstead, Appl. Phys. Lett. 88 (2006) 181903.